Int. J. Electrochem. Sci., 15 **(2020)** 9428 – 9445, doi: 10.20964/2020.09.63

International Journal of
ELECTROCHEMICAL
SCIENCE
www.electrochemsci.org

Study of the Cement Hydration Processes in Coal Metakaolin and Cement Blends by Electrochemical Impedance Spectroscopy

Shiwei Niu[1], *Pengju Han*[1*], *Funan Sun*[1], *Ruizhen Xie*[2], *Bin He*[1*], *Fuli Ma*[1], *Xingan Guo*[1], *Atiq Abdul Fattah*[1]

[1] College of Civil Engineering, Taiyuan University of Technology, Taiyuan, 030024, China
[2] Mechanics Institute, Jinzhong University, Jinzhong, 030619, China
[*]E-mail: 13834569544@163.com; hebin@tyut.edu.cn

Received: 31 May 2020 / *Accepted:* 13 July 2020 / *Published:* 10 August 2020

The hydration process of cement materials with coal metakaolin (CMK) was investigated by electrochemical impedance spectroscopy (EIS) using a new equivalent circuit model in this study. The results suggested that the electrochemical impedance characteristics of blended cement materials vary significantly with the content of CMK. The impedance parameters R_s and R_{ct1} associated with the changes in the cement microstructure increased with increasing hydration time and CMK content across the entire hydration process. Additionally, the fractal dimension d, which characterizes the complexity and density of the pore structure, showed a trend similar to those of the above impedance parameters, but the fractal dimension d_s, which characterizes the surface properties of the pore structure, showed the opposite trend. In addition, there was a significant correlation between the impedance parameter R_{ct1} and the compressive strength of the blended cements with different CMK contents and hydration times.

Keywords: hydration process; electrochemical impedance spectroscopy; coal metakaolin; compressive strength

1. INTRODUCTION

Supplementary materials, which are widely applied in cement production processes, reduce production costs and promote waste utilization [1-3]. The application of supplementary materials dates back to the mid-20th century, and a considerable amount of successful research was performed on these materials in the past few decades [4]. These studies demonstrated that supplementary materials can effectively improve the performance of blended cement materials through filling effects, pozzolanic effects and morphological effects [5-6]. Therefore, blended cement typically outperforms ordinary Portland cement. However, there are some limitations to these supplementary materials in applications.

For example, slag can induce the alkali-aggregate reaction in concrete [7], fly ash usually weakens the early strength of blended cement, and silica fume not only leads to high cost but also causes secondary pollution [8]. Therefore, it is essential and urgent to explore other effective supplementary materials for blended cement.

Coal metakaolin (CMK) is a new high-performance supplementary material that is formed by calcining coal kaolinite at a certain temperature [9]. Currently, CMK is mainly used in various industrial areas and has received some attention in the construction field as a supplementary material [10]. CMK can improve cement blend performance through both physical and chemical effects. In terms of physical effects, under a scanning electron microscope, CMK presents an irregular laminated structure, and its particle size distribution range is 0.1-5 μm [11]. The improvement in the cement blend performance from CMK occurs because this material can not only fill the pores between hydration products but also blend with the hydration products to construct a physical cross-linking network. In terms of chemical effects, the components of CMK are mainly Al_2O_3 and SiO_2, with a molar ratio of SiO_2/Al_2O_3 close to 2 [12]. Furthermore, owing to thermodynamic instability, CMK has relatively high pozzolanic activity, which can change the hydration process of blended cement. The change in the hydration process has a direct impact on the composition and micromorphology of the hydration products, which makes the interface between the hydration products denser. Additionally, the fineness and composition of CMK can affect the cement hydration process [13].

Hydration, a complex physicochemical process, is essential for cement materials because it determines the microstructure of these materials and then affects their macro-performance [14-15]. Much research work has been done on cement hydration by various testing methods. In the case of persistent hydration reactions, the isothermal calorimetry method is widely employed [16-17]. In the analysis of hydration products, scanning electron microscopy (SEM) [18-19], X-ray diffraction (XRD) [20-21] and Fourier transform infrared spectroscopy (FTIR) [22] are the most commonly used methods. These methods, however, cannot provide real-time nondestructive monitoring of the cement hydration process. Some testing methods that can monitor the hydration process in real time and are nondestructive have been proposed [23-24]. In this study, electrochemical impedance spectroscopy (EIS), the most widely used nondestructive testing method, is adopted [25]. Because cement materials can be considered to be a special electrochemical system [26-27], EIS can be used to investigate the cement hydration process. Furthermore, EIS has advantages in monitoring the microstructure changes of cement materials under different conditions and environments [28].

The purpose of this research is to investigate the hydration process of cement materials with CMK by monitoring the electrochemical impedance behavior of these materials. The influence of CMK on the cement hydration process is analyzed, and the microstructure changes in blended cement materials are discussed using the impedance parameters. The microstructure changes in cement materials with CMK are also discussed in terms of the fractal dimension. Then, the correlation between the electrochemical impedance parameter (R_{ct1}) and the compressive strength is established, and the influence of the CMK content on this correlation is analyzed.

2. MATERIALS AND EXPERIMENTS

2.1 Experimental materials

High belite sulfoaluminate cement (HBSC) with a strength grade of 42.5 from the Polar Bear Material Company in Tangshan, China, was used in the tests. HBSCs are an attractive class of new cement materials that have the characteristics of low energy consumption and low CO_2 emission during the production process [29-30]. CMK, from the Ju Feng Kaolin Company in Datong, China, was used as the supplementary material. The chemical composition and mineralogical composition of the HBSC are presented in Table 1 and Table 2 respectively. In the chemical composition of the CMK, SiO_2 accounts for 51.0% of the mass ratio, while Al_2O_3 accounts for 44.66% of the mass ratio, and the rest of the components are impurities. The specific chemical composition of the CMK is shown in Table 3. Normal tap water was used in the experiment, and there were no other admixtures.

Table 1. Chemical composition of HBSC

Chemical composition	CaO	SiO_2	Al_2O_3	Fe_2O_3	MgO	SO_3	TiO_2	Sum	Loss
Mass (%)	51.54	13.80	15.34	1.52	2.08	14.21	0.71	99.20	0.38

Table 2. Mineralogical composition of HBSC

Mineralogical composition	$C_4A_3\bar{S}$	C_2S	f-$CaSO_4$	C_4AF	f-CaO	CT
Mass (%)	29.35	38.06	13.64	5.08	1.84	1.11

Table 3. Chemical composition of CMK

Chemical composition	SiO_2	Al_2O_3	Fe_2O_3	TiO_2	CaO	MgO	K_2O	Na_2O	Loss
Mass (%)	51.0	44.66	0.96	1.89	0.37	0.24	0.28	0.55	0.05

2.2 Test procedure

The specimens were prepared with CMK contents of 0%, 10%, 20%, and 30%. The water-cement ratio of all specimens was 0.6. The specimens for the EIS tests were cast into molds with dimensions of 70.7mm×70.7mm, while the specimens for the compressive strength tests were cast into molds with dimensions of 40mm×40mm×160mm. All specimens were stored in a curing chamber (95±5% RH, 20±2℃) until the specified time.

The CS350 electrochemical workstation was used to monitor the electrochemical impedance behavior of cement materials with different hydration times (1 d, 3 d, 7 d, 14 d, 21 d, and 28 d). To improve the measurement accuracy, the tests adopt an automatic bias to eliminate the potential and current. According to “Method of testing cements-Determination of strength” (GBT 17671-1999), a

compression-testing instrument (WDW-100) was used for the compressive strength tests of the samples with different hydration times (1 d, 7 d, 14 d, 21 d, and 28 d).

3. RESULTS AND ANALYSIS

3.1 Analysis of Nyquist plots

As shown in Figure 1, the EIS results are analyzed in the form of Nyquist plots, with both the imaginary part (Z'') and real part (Z') of the impedance considered. The electrochemical impedance curves in the Nyquist plot in different hydration periods show apparently different characteristics, which is helpful for distinguishing the hydration process [31-32].

From the Nyquist plots of the blended cements with different CMK contents and hydration for 1 d, shown in Figure 1(a), the impedance curve is basically a straight line, without a semicircle in the high frequency region. This shows that there are no obvious electrochemical reactions in the cement materials. It is well known that the electrochemical reaction can only occur on the rough surface of the hydrated calcium silicate gel and can only proceed when the hydrated calcium silicate gel has accumulated to a certain amount [33]. Therefore, the hydration degree of dicalcium silicate (C_2S) is still low after 1 d of hydration, and only a small amount of hydrated calcium silicate gel is generated, which is far from sufficient for a significant electrochemical reaction.

With the progress of cement hydration, the hydration degree of C_2S gradually increases, and a certain amount of hydrated calcium silicate gel accumulates in the cement material. As a result, the electrochemical reaction can proceed normally, and the formation of a connected pore structure within the blended cement is initiated. At 3 d of hydration, as shown in Figure 1(b), the impedance curves begin to shift toward quasi-Randles curves but with no obvious curve characteristics. Compared with other supplementary materials, CMK significantly accelerated the hydration process of cement [27]. Correspondingly, in the high frequency region a certain degree of curvature is exhibited, while in the low frequency region, a straight line with an inclination less than 45° is present.

After 7 and 14 d of hydration, as shown in Figure 1(c) and 1(d), the impedance curves have typical quasi-Randles curve features. In the high-frequency region, a certain degree of curvature is exhibited that is more complete than that at 3 d of hydration. In the low frequency region, a straight line is present with an inclination value smaller than that of the previous hydration period. In addition, the shape of the impedance curves varies significantly with changing CMK content. For the same hydration period, the higher the content of CMK is, the more complete the high frequency curve. However, for other supplementary materials, the impedance curve of the blended cement begins to show quasi-Randles characteristics at this stage [34]. To some extent, this indicates that CMK can promote the process of cement hydration and produce more hydration products.

Figure 1(e) shows the Nyquist plots of the blended cements after 28 d of hydration. Compared with the impedance curves at 14 d of hydration, the shape of the impedance curves in the high frequency region remains almost unchanged, with only a slight change in the position and semicircle diameter of the impedance curve; the low frequency region still exhibits a straight line but with a smaller inclination.

This occurs because the hydration is in a stable state and a complete and connected capillary network has been formed inside the cement materials. In the high-frequency region, the impedance curves of the blended cements with different CMK contents are more complete than those of the cement materials without CMK, and the impedance curves of the CMK contents of 20% and 30% tend to be consistent. In the low frequency region, as the CMK content increases, the slope of the straight line tends to decrease, indicating that the structure of the cement material becomes dense and ion diffusion is difficult [34].

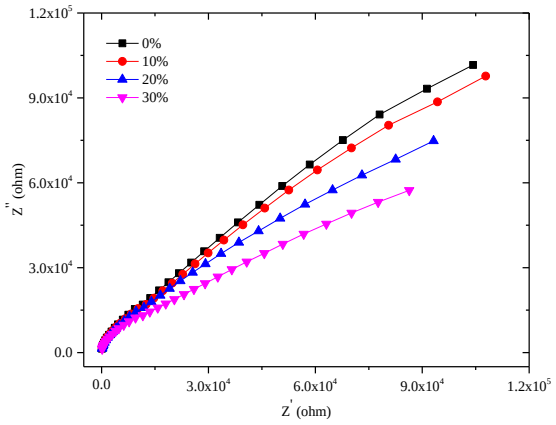

(a) 1 d

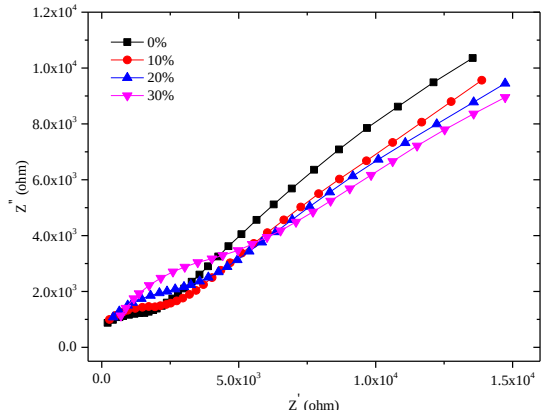

(b) 3 d

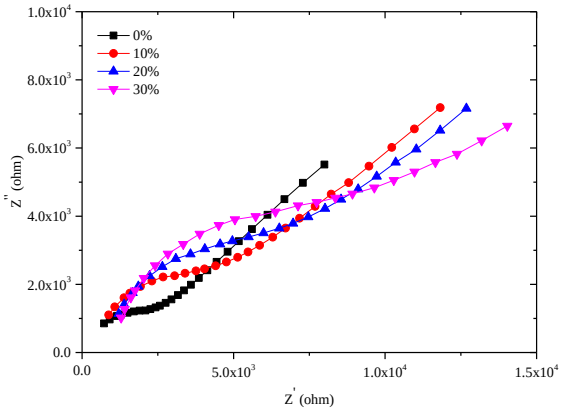

(c) 7 d

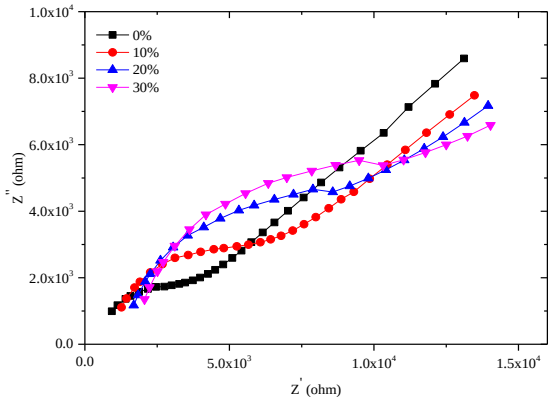

(d) 14 d

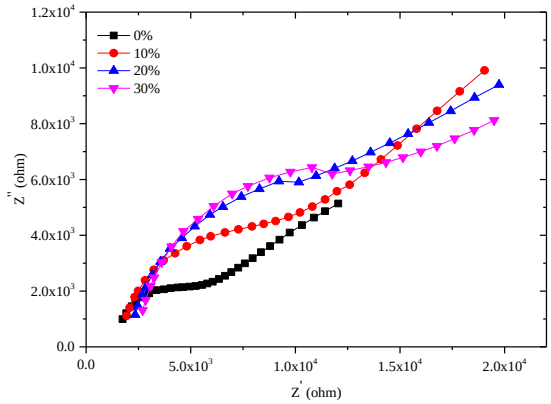

(e) 28 d

Figure 1. The Nyquist plots for different hydration periods

3.2 Equivalent circuit model

3.2.1 Presentation of a novel EC model

The equivalent circuit method is widely used in the analysis and application of EIS. In this method, the impedance curve is analyzed by the equivalent circuit (EC) model, which is composed of series and parallel elements such as capacitance, inductance and resistance, and the characteristics of the electrochemical system are characterized by the obtained element parameters. Many existing EC models are used to analyze the cement hydration process, such as the typical EC model, which is described as R_s (CPE_1($R_{ct1}W_1$)) (shown in Figure 2(a)) [35], and Dong's EC model, which is described as R_s (C_1($R_{ct1}W_1$))(C_2($R_{ct2}W_2$)) (presented in Figure 2(b)) [36-37]. However, these EC models suffer from a number of limitations. For example, the typical EC model ignores the Faraday process between the electrode and the cement material interface; Dong's EC model does not take into account the effects of dispersion [38-39]. Therefore, as shown in Figure 2(c), a novel equivalent circuit model that is more suitable for characterizing the hydration process of blended cement, described as R_s (CPE_1 ($R_{ct1}W_1$)) (CPE_2 ($R_{ct2}W_2$)), is proposed. We consider the dispersion effect as well as the Faraday process between the electrode and the cement material interface in the proposed model.

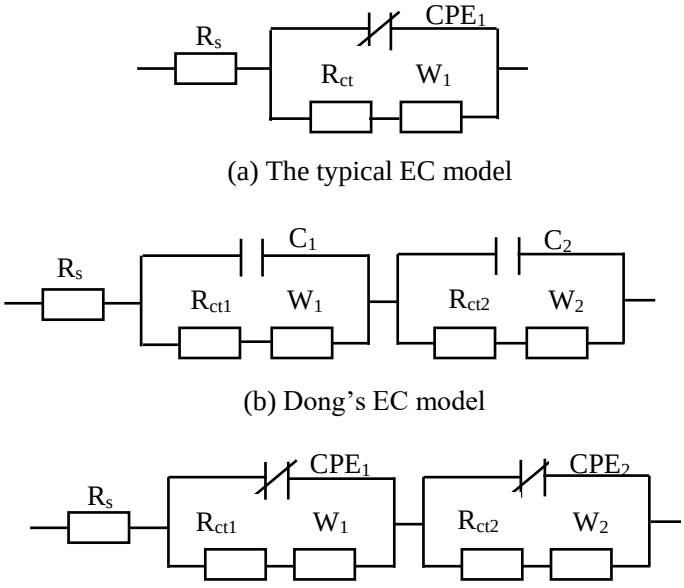

Figure 2. Equivalent circuit models

The significance of each parameter in these models is as follows: R_s is the electrolyte resistance in the pore solution; CPE_1 is the constant phase element that represents the electrical double layer capacitance between the solid phase and the liquid phase in the cement specimen; R_{ct1} is the resistance of the charge transfer process in the cement specimen; W_1 is the Warburg resistance of the diffusion process in the cement specimen; C_1 is the electrical double layer capacitance between the solid phase and the liquid phase in the cement specimen; C_2 is the electrical double layer capacitance between the cement specimen and the electrode; CPE_2 is the constant phase element that represents the electrical double layer capacitance between the cement specimen and the electrode; R_{ct2} is the resistance of the charge transfer process between the cement specimen and the electrode; and W_2 is the Warburg resistance of the diffusion process on the electrode surface.

CPE is a special electrochemical element, and the corresponding mathematical expression is shown in Eq. (1).

$$Z = Y \cdot \omega^{-n} \cdot (\cos\frac{n\pi}{2} - j\sin\frac{n\pi}{2}) \tag{1}$$

Z is the impedance of the CPE; Y is the admittance of the constant phase element; ω is the angular frequency; and n is the constant phase index.

The impedance mathematical expression of the proposed equivalent circuit model in this study is shown in Eq. (2).

$$Z = R_s + \frac{Y_1\omega^{-n}\left[\cos(n\pi/2) - j\sin(n\pi/2)\right]\left[R_{ct1} + \sigma_1\omega^{-1/2}(1-j)\right]}{Y_1\omega^{-n}\left[\cos(n\pi/2) - j\sin(n\pi/2)\right] + \left[R_{ct1} + \sigma_1\omega^{-1/2}(1-j)\right]} + \frac{Y_2\omega^{-n}\left[\cos(n\pi/2) - j\sin(n\pi/2)\right]\left[R_{ct2} + \sigma_2\omega^{-1/2}(1-j)\right]}{Y_2\omega^{-n}\left[\cos(n\pi/2) - j\sin(n\pi/2)\right] + \left[R_{ct2} + \sigma_2\omega^{-1/2}(1-j)\right]} \tag{2}$$

Y_1 is the admittance of the constant phase element CPE_1; σ_1 is the diffusion impedance coefficient of W_1; Y_2 is the admittance of the constant phase element CPE_2; and σ_2 is the diffusion impedance coefficient of W_2.

3.2.2 Validation of the EC model

To validate the novel model and demonstrate its applicability, the Nyquist plots of the blended cement materials (CMK content =20%) at hydration periods of 1 d, 7 d and 28 d are fitted by the proposed model. As shown in Figure 3 (a), 3(b) and 3(c), the fitting results are basically consistent with the experimental points. Thus, the proposed model is suitable for investigating the hydration process of CMK cement.

The novel model is also verified by fitting the typical EC model and Dong's EC model with the Nyquist plot of the CMK cement (CMK content = 20%) at 28 d of hydration. As shown in Figure 3 (d) and 3 (e), the fitting results of the typical model in the low frequency region deviate from the impedance curve to some extent; conversely, the fitting results of Dong's model in the high frequency region are closer to a semicircle and deviate from the impedance curve. Therefore, the proposed model performs better than the other two models.

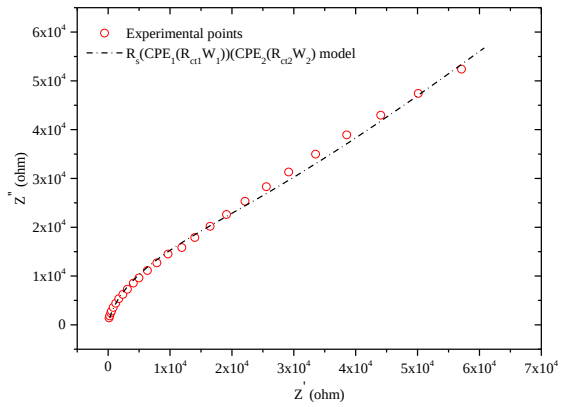

(a) 1 d

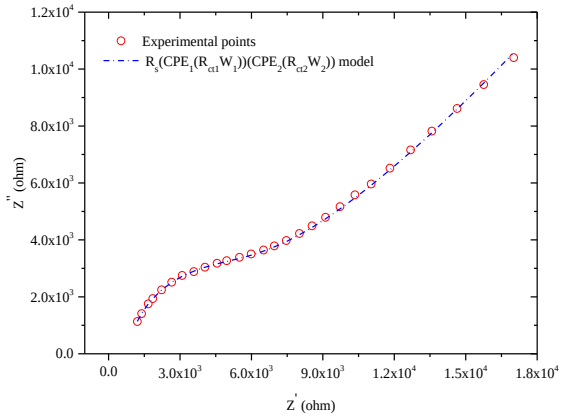

(b) 7 d

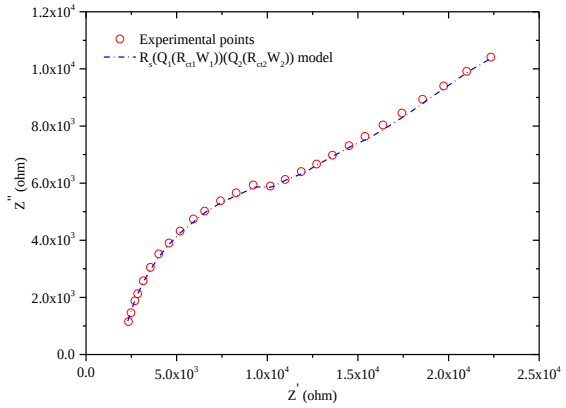

(c) 28 d

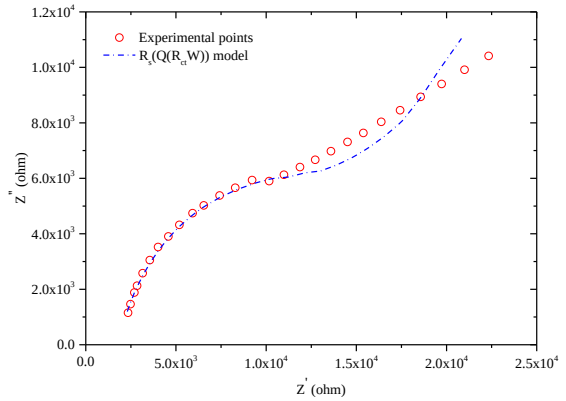

(d) The typical model

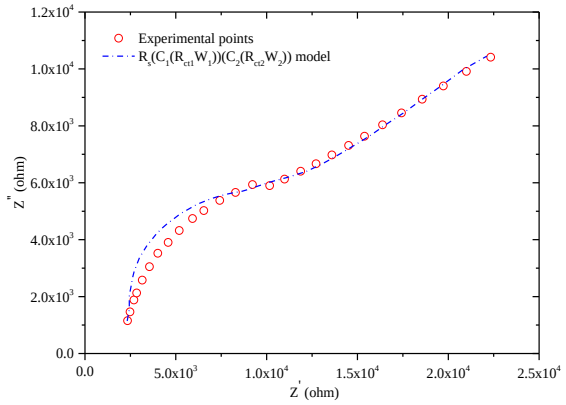

(e) Dong's model

Figure 3. The model fitting results for the blended cement

3.3 Analysis of the impedance parameters

Based on the proposed equivalent circuit model, the Nyquist plots of the cement materials with different CMK contents and hydration times are fitted to obtain the impedance parameter values. The microstructure characteristics, which are closely related to the mechanical properties of cement materials, are the focus of the research on the cement hydration process. Among the parameters of the proposed equivalent circuit model, the impedance parameters R_s and R_{ct1} are sensitive to the

microstructure changes of cement materials. Therefore, the microstructure changes of cement materials during the hydration process are discussed using the above two parameters.

3.3.1 Impedance parameter R_s

The values of the impedance parameter R_s of the cement materials with different hydration periods and different CMK contents are shown in Table 4 and Figure 4. This parameter is determined by both the total concentration of ions and the total porosity [40-41]. Theoretically, as the hydration time increases, the total ion concentration in the pore solution increases significantly, and the parameter value should decrease greatly. However, as seen from the figure, the parameter value shows an increasing trend with increasing hydration time, and the increase rate gradually decreases with the progress of hydration. The increasing trend of the parameter value occurs because when the hydration reaches a certain level, generally 1 d-2 d, the total ion concentration in the pore solution tends to be constant, while the total porosity decreases continuously due to the hydration products occupying the internal pores [34][42]. That is, of the two factors that determine the parameter value, the factor of the total porosity plays a predominant role. The increase rate of the parameter value decreases because there is less space available for the cement hydration products to fill with the hydration process, and the rate of decrease in the porosity decreases.

It can also be observed that the impedance parameter R_s of the cement materials that incorporate different CMK contents are all greater than those of the cement materials without CMK for the same hydration period, and the parameter values increase with increasing CMK content. This is inconsistent with the literature results that the parameter R_s of fly ash cement decreases with the increase of fly ash content in the early stage of hydration [34]. The main reasons for these phenomena are threefold. (1) CMK exerts filling and densification effects [39-40] that can impede the ion transport in the pore solution. (2) The substitution of part of the cement with CMK not only increases the water-cement ratio but also decreases the total ion concentration in the pore solution. (3) CMK can promote the cement hydration process, which increases the amount of hydration products and thus decreases the porosity. This conclusion is consistent with the research results that CMK can promote cement hydration [42].

Table 4. The values of the impedance parameter R_s for different hydration periods

Content	Impedance parameter R_s/(ohm)					
	1 d	3 d	7 d	14 d	21 d	28 d
0%	107	214	723	931	1340	1745
10%	113	282	877	1267	1482	1937
20%	153	419	1209	1689	2300	2345
30%	177	698	1289	2065	2446	2700

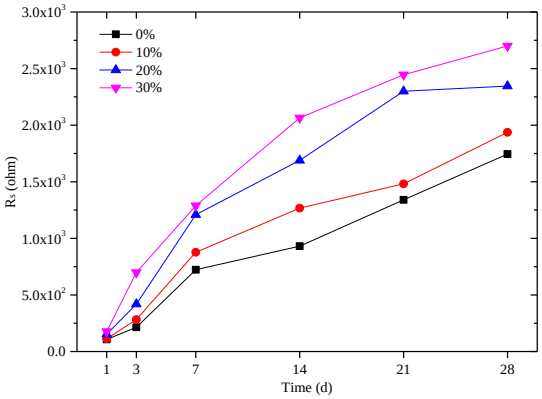

Figure 4. The values of the impedance parameter R_s for different hydration periods

3.3.2 Impedance parameter R_{ct1}

The high-frequency semicircle in the Nyquist plot reflects the characteristics of the charge transfer process, and the diameter of the semicircle is the impedance parameter (R_{ct1}) [43]. The increase in the impedance parameter value essentially reflects the densification of the microstructure of cement material. The values of the impedance parameter R_{ct1} of the blended cement materials with different hydration periods and different CMK contents are shown in Table 5 and Figure 5. The R_{ct1} values are very small after 1 d of hydration due to the low degree of hydration, which is consistent with the results in the literature [34]. Then, the value of R_{ct1} increases rapidly because the space inside the cement material is quickly filled with hydration products, which leads to a decrease in the porosity and the densification of the microstructure. After 7 d -14 d of hydration, the increase in the R_{ct1} value is slower because the space that the hydration products can fill decreases. Therefore, the R_{ct1} value increases continuously throughout the hydration process, while the microstructure becomes increasingly dense.

Additionally, the parameter values of the cement materials that incorporate different CMK contents are all greater than those of the cement materials without CMK over the same period, and the parameter values increase with increasing CMK content. However, in the literature, the R_{ct1} value of the cement materials with small amount of fly ash is greater than those of the cement materials with large amount of fly ash in the early hydration stage, and the R_{ct1} value of the cement materials increases with the increase of fly ash content until the later stage of hydration [34]. These results occur because fly ash has only filling effect in the early hydration stage, and the second hydration reaction of fly ash does not appear until the late hydration stage, while CMK not only has a filling effect but also accelerates the hydration progress of cement throughout the hydration process [34][42]. Furthermore, as the hydration time increases, the increase in the parameter value with increasing CMK content is more significant. With increasing CMK content, more fine particles fill the pores, and the amount of hydration products increases over the same period, which increases the compactness of the cement material microstructure and makes ion transport in the pore solution more difficult.

Table 5. The values of the impedance parameter R_{ct1} for different hydration periods

Content	Impedance parameter R_{ct1}/(ohm)					
	1 d	3 d	7 d	14 d	21 d	28 d
0%	401	914	1941	3062	3527	4452
10%	537	1678	3960	7423	7732	8054
20%	761	2347	5521	8487	9849	11300
30%	1071	3708	8984	10650	11227	12090

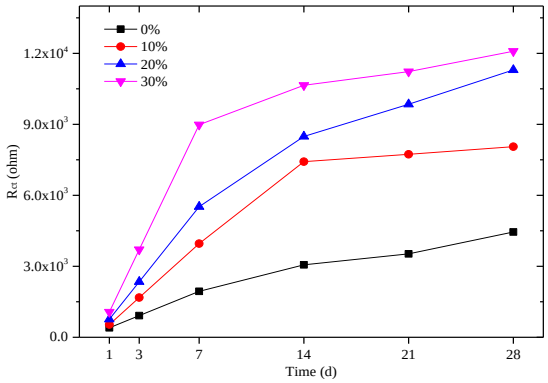

Figure 5. The values of the impedance parameter R_{ct1} for different hydration periods

3.4 Analysis of fractal dimension

There are two impedance parameters in the established equivalent circuit model of cement materials, electrical double layer capacitance C_d and Warburg resistance W. These two impedance parameters respectively represent pore surface properties and pore volume properties, which can use as a window to investigate the pore structure changes of cement materials. The position of the two impedance parameters in the equivalent circuit is different, so they can be separated well [44]. However, the above two impedance parameters are not direct indicators of the microstructure of cement materials, and the corresponding index obtained by these parameters has a quantitative relationship with fractal dimension. Therefore, this research provides a method to obtain the complete microstructure of cement materials by electrochemical impedance spectroscopy. There are two existing fractal dimensions: the pore surface fractal dimension d_s and the pore volume fractal dimension d.

3.4.1 Fractal dimension d_s

The fractal dimension d_s is closely related to the pore structure parameters of cement materials. The smaller the fractal dimension d_s is, the smaller the average pore size and median pore size, and the denser the structure of the cement material. The electrical double layer capacitance C_{d1} is replaced by a constant phase element, which is expressed as $C_{d1}=K\ (j\omega)^{-q}$, and the constant phase index q reflects the flattening degree of the high frequency semicircle. There is a quantitative relationship between the fractal

dimension d_s and the constant phase index q, which is expressed as d_s=3-q [45]. The values of the constant phase index q and fractal dimension d_s of the blended cement materials with different CMK contents are shown in Table 6.

The range of fractal dimension d_s values is between 2.090-2.214, which is different from the literature results [45]. This occurs because the value of fractal dimension d_s is greatly affected by factors such as cement type and supplementary material type. As the hydration time increases, the value of the element index q increases, and the value of the fractal dimension d_s decreases accordingly. This indicates that during the hydration process, the number of small pores increases, the number of large pores decreases, and the pore size distribution is optimized. This is consistent with the literature results [34]. After 28 d of hydration, the d_s value of the cement materials with different CMK contents is close to 2.

The value of q increases with increasing CMK content over the same hydration period, and the value of d_s decreases accordingly. Moreover, the values of q and d_s vary greatly during the entire hydration process, which is different from the literature result that the value of q is approximately 1[46]. These results occur because CMK has a stronger filling effect and pozzolanic effect than other supplementary materials. Therefore, CMK can not only accelerate the cement hydration process but also generate more hydration products, thereby reducing the porosity, average pore size and pore size distribution of cement materials.

Table 6. The values of the constant phase index and fractal dimension

Hydration time (d)	0%		10%		20%		30%	
	q	d_s	q	d_s	q	d_s	q	d_s
1	0.786	2.214	0.787	2.213	0.791	2.209	0.792	2.208
3	0.808	2.192	0.809	2.191	0.817	2.183	0.821	2.179
7	0.825	2.175	0.824	2.176	0.832	2.168	0.834	2.166
14	0.835	2.165	0.836	2.164	0.839	2.161	0.840	2.160
21	0.854	2.146	0.869	2.131	0.872	2.128	0.878	2.122
28	0.879	2.121	0.888	2.112	0.899	2.101	0.910	2.090

3.4.2 Fractal dimension d

The fractal dimension d is a parameter for characterizing the complexity and density of the pore structure. There is a quantitative relationship between the parameter d and the index p [47], which is expressed as d=4-p, and the index p can be obtained from the angle between the low frequency straight line and the real axis, that is, the angle divided by $\pi/2$ is the value of the index p. The values of index p and fractal dimension d of the blended cement materials with different CMK contents are shown in Table 7. The range of pore volume fractal dimension d values is between 3.512-3.786, which is larger than the fractal dimension of fly ash cement (3.3-3.5) and coal fractal dimension (2.6-2.75) in the literature [48]. The reason may be related to the pore structure characteristics of the material. From the viewpoint of fractal theory, when the fractal dimension is greater than 3, it shows that the distribution pattern of the pores is quite complex and irregular, and only the fractal dimension can describe its spatial distribution.

The physical significance of the increase in the fractal dimension is that the porosity and average pore size decrease, and the number of small pores increases, while the number of large pores decreases, which refines and optimizes the pore structure. Generally, the pore volume fractal dimension of the hydration product will increase with the increase of the hydration time, and increase with the increase of the content of supplementary materials [47-48]. The variation of pore volume fractal dimension of CMK content hydration product with hydration time and supplementary material content is investigated. The value of pore volume fractal dimension d increases with increasing hydration time, which is consistent with the results of mercury intrusion porosimetry (MIP) in the literature [48]. This shows that as hydration progresses, the pore structure of cement material is optimized, and the microstructure becomes dense. However, the value of the pore volume fractal dimension increases with increasing CMK content over the same hydration time, which is different from the literature results. This occurs because CMK has higher pozzolanic effect than other supplementary materials, so the hydration process of cement materials is accelerated with the increase of CMK content.

Table 7. The values of the element index and fractal dimension

Hydration time (d)	0%		10%		20%		30%	
	p	d	p	d	p	d	p	d
1	0.488	3.512	0.386	3.614	0.372	3.628	0.327	3.673
3	0.448	3.552	0.381	3.619	0.348	3.652	0.325	3.675
7	0.432	3.568	0.373	3.627	0.337	3.663	0.323	3.677
14	0.404	3.596	0.357	3.643	0.302	3.698	0.289	3.711
21	0.371	3.629	0.312	3.688	0.268	3.732	0.234	3.766
28	0.337	3.663	0.287	3.713	0.229	3.771	0.214	3.786

3.5 Compressive strength

The impedance parameter R_{ct1} is sensitive to the microstructure changes of cement materials and is the main indicator for investigating the microstructure changes [49-50]. The microstructure changes are closely related to the mechanical properties, especially the compressive strength. Thus, this study aims to establish the relationship between the impedance parameter R_{ct1} and the compressive strength. As shown in Table 8 and Figure 6, the compressive strength shows a growth trend similar to that of the impedance parameter R_{ct1}. At the beginning of the test, the compressive strength increases sharply because the hydration products quickly fill the pores in the early stage of hydration, resulting in a rapid decrease in porosity. After 14 d of hydration, the increase in compressive strength slows because there is less space for the hydration products to fill. Overall, there is an increase in the compressive strength as hydration progresses. This is consistent with the increasing trend of strength of slag cement and kaolin cement in the literature [27]. Additionally, the compressive strength of the cement materials in the same period increases with increasing CMK content. This occurs because with the increase of CMK content, the average pore size, median pore size and porosity of cement materials decrease, which improves the compactness of cement materials and refines its pore structure [48].

Table 8. Compressive strength of cement materials with different CMK contents and hydration times

Content	Compressive strength/(MPa)				
	1 d	7 d	14 d	21 d	28 d
0%	6.45	18.49	29.38	41.34	45.80
10%	7.32	21.51	40.93	49.92	52.01
20%	9.97	35.83	41.32	53.43	59.13
30%	13.94	41.78	59.02	62.21	65.93

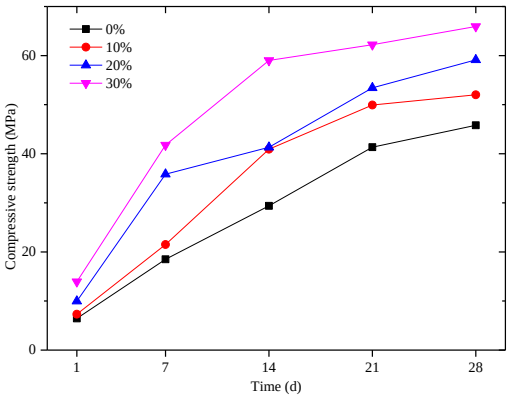

Figure 6. Compressive strength of cement materials with different CMK contents and hydration times

The correlation between the impedance parameter R_{ct1} and the compressive strength of the cement materials with different CMK contents is analyzed. As shown in Figure 7, a linear equation (y = ax + b) is proposed to fit the relationship between the compressive strength and the impedance parameter R_{ct1}. All the correlation coefficients, R^2, are greater than 0.94, indicating a significant correlation between the two parameters. The slope of the fitting curve decreases with increasing CMK content, while the slopes of the fitting curve for the blended cements with CMK contents of 20% and 30% are almost the same. The intercept of the fitting curve reaches the maximum value when the CMK content in the blended cement is 20%. Therefore, based on the novel equivalent circuit model, it is feasible to predict the compressive strength of cement materials with the fitting parameter R_{ct1} according to electrochemical impedance spectroscopy.

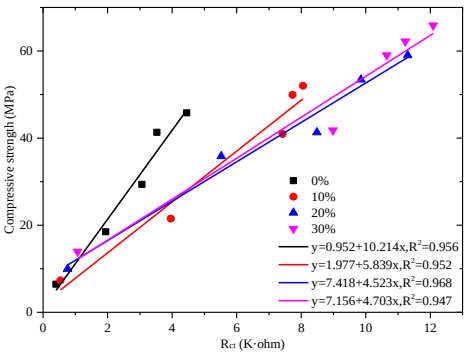

Figure 7. The correlation between the compressive strength and the impedance parameter R_{ct1} for the cement materials

4. CONCLUSIONS

In this study, the influence of CMK on the hydration process of cement materials was investigated by electrochemical impedance spectroscopy with a novel equivalent circuit model. The impedance parameter and fractal dimension associated with the microstructure changes of blended cement materials were analyzed. The following conclusions were obtained:

1) The CMK incorporation changed the hydration process of the cement materials. The diameter of the high-frequency semicircle of the cement materials increased with increasing CMK content during the entire hydration process. In addition, the Nyquist plots with different hydration times had their own curve characteristics. Since there were no obvious electrochemical reactions, the high frequency region of the1 d hydration was a straight line. With the process of hydration, the curve in the high frequency region acquired a certain curvature. After 28 d of hydration, the curve in the high frequency region was a flattened semicircle.

2) A novel equivalent circuit model considering the dispersion effect as well as the Faraday process between the electrode and the cement material interface was proposed. The fitting results of different hydration times demonstrated that the proposed model is suitable for investigating the entire hydration process of CMK cement. Compared with those of the other two models, the fitting curves of the proposed model were more consistent with the experimental results.

3) The impedance parameters R_s and R_{ct1} of the cement materials increased with increasing CMK content and hydration time across the entire hydration process. This indicated that CMK incorporation reduced the total porosity of the cement materials and made the microstructure dense. The fractal dimension d that characterizes the volume properties of the pore structure showed a trend similar to those of the impedance parameters, but the fractal dimension d_s that characterizes the surface properties of the pore structure was the opposite.

4) The compressive strength showed a similar growth trend to that of the impedance parameter R_{ct1}. The impedance parameter R_{ct1} and the compressive strength were significantly correlated, this relationship was fitted with a linear equation, and all of the correlation coefficients were greater than 0.94. Thus, it is feasible to nondestructively monitor the compressive strength of blended cement materials using the impedance parameter R_{ct1}.

ACKNOWLEDGEMENTS

The authors would like to acknowledge the financial support provided by the National Natural Science Foundation of China (No. 41807256/51208333), the Special Talent Project of Shanxi Province (Science and Technology Innovation Project for Outstanding Talents 2019), phD research launch project of Jinzhong University, Scientific and technological innovation projects of colleges and universities in Shannxi Province and Opening project of Sichuan University of Science and Engineering, Material Corrosion and Protection Key Laboratory of Sichuan Province(No. 2020CL13).

References

1. B. Lothenbach, K. Scrivener and R.D. Hooton, *Cem. Concr. Res*., 41(3) (2011) 217.

2. F. Saly, L.P. Guo, R. Ma, C.P. Gu and W. Sun, *J. Wuhan Univ. Technol. (Mater. Sci. Ed.),* 33(6) (2018) 1444.
3. S.K. Patel, R.K Majhi, H.P. Satpathy and A.N. Nayak, *Constr. Build. Mater*., 226(2019) 579.
4. K.H. Mo, T.C. Ling, U.J. Alengaram and S.P. Yap, *Constr. Build. Mater*., 139 (2017) 403.
5. H. Toutanji, N. Delatte, S. Aggoun, R. Duval and A. Danson, *Cem. Concr. Res.,* 32(2) (2004) 311.
6. Ashish and D. Kumar, *J. Clean. Prod*., 211 (2019) 716.
7. E. Crossin, *J. Clean. Prod.,* 95 (2015) 101.
8. O. Tan, G. Gungormus and A.S. Zaimoglu, *KSCE J. Civ. Eng*., 18(6) (2014) 1650.
9. L.H. Wang, X.Y. Li, Y. Cheng and X.H. Bai, *Constr. Build. Mater*., 166 (2018) 592.
10. X.M. Du, Q.F. Liu and N. Xing, Metal *Mine,* 9 (2010) 170.
11. Y.F. Deng, X.B. Yue and S.Y. Liu, *Eng. Geol*., 193 (2015) 146.
12. L.E. Gordon, R.S. Nicolas and J.L. Provis, *Int. J. Greenh. Gas Con*., 27(8) (2014) 255.
13. E. Berodier and K. Scrivener, *Cem. Concr. Res*., 73 (2015) 25.
14. K.L. Scrivener and A. Nonat, *Cem. Concr. Res*., 41(7) (2011) 651.
15. K. Svinning, A. Høskuldsson and H. Justnes, *Cem. Concr. Comp*., 30(2) (2012) 138.
16. L. Pelletier, F. Winnefeld and B. Lothenbach, *Cem. Concr. Comp*., 32(7) (2010) 497.
17. X.Y. Pang, D.P. Bentz, C. Meyer, G.P. Funkhouser and R. Darbe, *Cem. Concr. Comp*., 39(5) (2013) 23.
18. B. Gaël, T. Christelle, E. Gilles, G. Sandrine and S.F. Tristan, *Constr. Build. Mater*., 126 (2016) 157.
19. N. Chitvoranund, F. Winnefeld, C.W. Hargis, S. Sinthupinyo and B. Lothenbach, *Adv. Mater. Res*., 29(3) (2017) 101.
20. J.W. Bullard, H.M. Jennings, R.A. Livingston, A. Nonat, G.W. Scherer, J.S. Schweitzer, K.L. Scrivener and J.J. Thomas, *Cem. Concr. Res.,* 41(12) (2010) 1208.
21. A. Rungchet, C.S. Poon, P. Chindaprasirt and K. Pimraksa, *Cem. Concr. Comp*., 83 (2017) 10.
22. A. Guerrero, A. María, M. Gutiérrez and Ruby, *Constr. Build. Mater*., 193 (2018) 518.
23. J.R. Zhang, T.Y. Fan, H.Y. Ma and Z.J. Li, *Constr. Build. Mater*., 88 (2015) 118.
24. S.W. Tang, X.H. Cai, Z. He, W. Zhou, H.Y. Shao, Z.J. Li, T. Wu and E. Chen, *Constr. Build. Mater*., 146 (2017) 15.
25. T. Pajkossy and R. Jurczakowski, *Curr. Opin. Electrochem*., 1(1) (2017) 53.
26. B.Q. Dong, J.C. Zhang, Y.Q. Liu, G.H. Fang, Z. Ding and F. Xing, *Constr. Build. Mater*., 113 (2016) 997.
27. B.Q. Dong, G. Li, J.C. Zhang, Y.Q. Liu, F. Xing and S.X. Hong, *Constr. Build. Mater*., 149 (2017) 467.
28. B.Q. Dong, Q.W. Qiu, J.Q. Xiang, C.J. Huang, X. Feng and N.X. Han, *Mater*., 7(1) (2014) 218.
29. E. Gartner and T. Sui, *Cem. Concr. Res*., 114 (SI) (2018) 27.
30. M.Z Lan, B.F. Xiang, J. Zhou, Z.X. Ge and C.J. Liu, *B. Chin. Ceram. Soc*., 36 (8) (2017) 2720.
31. J.J. Thomas, J.J. Biernacki, J.W. Bullard, S. Bishnoi, J.S. Dolado, G.W. Scherer and A. Luttge, *Cem. Concr. Res*., 41 (2011) 1257.
32. F. Bullerjahn, E. Boehm-Courjault, M. Zajac, H.M. Ben and K. Scrivener, *Cem. Concr. Res*., 116 (2019) 1208.
33. M. Cabeza, P. Merino and A. Miranda, *Cem. Concr. Res*., 32 (2002) 881.
34. F.J. Jiang, J.X. Gong and W. Zha*ng, J.Xi'an Univ. of Arch.& Tech.,* 48(4) (2016) 493.
35. M.L. Shi, Z.Y. Chen and J. Sun, *Cem. Concr. Res.,* 29(7) (1999) 1111.
36. P. Gu, P. Xie, J.J. Beaudoinb and R. Brousseaub, *Cem. Concr. Res*., 23(1) (1993) 157.
37. P. Gu, P. Xie and J.J. Beaudoinb, *Cem. Concr. Res.,* 23(3) (1993) 581.
38. F.Q. He, R.P. Wang, C.J. Shi, R.X. Zhang, C.P. Chen, L. Lin and X.P. An, *Constr. Build. Mater*., 143 (2017) 179.
39. B.Q. Dong, Q.W. Qiu, J.Q. Xiang, C.J. Huang, F. Xing, N.X. Han and Y.Y. Lu, *Constr. Build. Mater.,* 54 (2014) 558.

40. H. Ma and Z. Li, *Comput. Concr*., 11(4) (2013) 317.
41. C. Çetin, S.T. Erdogan and M. Tokyay, *Cem. Concr. Comp*., 67 (2015) 39.
42. I. Janotka, F. Puertas and M. Palacios, *Constr. Build. Mater.,* 24(5) (2010) 791.
43. M.L. Shi, *Impedance Spectroscopy of Concrete*, China Railway Press, (2003) Beijing, China.
44. S.H. Shi and Z.Y. Chen, *J. Build. Mater*., 1(1)(1998) 30.
45. Y. Zhang, Z. Jin and Y. Zhang, *J. Chin. Ceramic Soc*., 45(2) (2017) 249.
46. S.S. Jin, J.X. Zhang and C.Z. Chen, *J. Build. Mater*., 14(1) (2011) 92.
47. X. Ji, S.Y.N. Chan and N. Feng, *Cem. Concr. Res*., 27(11) (1997) 1691.
48. Y.X. Li, Y.M. Chen, X.Y. He, J.X. Wei, W.S. Zhang, H.T. Zhang and S.H. Guo, J. Chin. Ceramic Soc., 31(8) (2003) 774.
49. M. Cabeza, M. Keddam, X.R. Novoa, I. Sanchez and H. Takenouti, *Electrochim. Acta*, 51 (2006) 8.
50. Z.Y. Liu, Y.S. Zhang and Q. Jiang, *Constr. Build. Mater*., 53(53) (2014) 26.